Journal of Magnetic Resonance 210 (2011) 184–191

Contents lists available at ScienceDirect

Journal of Magnetic Resonance

journal homepage: www.elsevier.com/locate/jmr

Anomalous NMR relaxation in cartilage matrix components and native cartilage: Fractional-order models ☆

Richard L. Magin [a,*], Weiguo Li [a], M. Pilar Velasco [b], Juan Trujillo [c], David A. Reiter [d], Ashley Morgenstern [d], Richard G. Spencer [d]

[a] Department of Bioengineering, University of Illinois at Chicago, Chicago, IL 60607, USA
[b] Departamento de Matematica Aplicada, Facultad de Matematicas, Universidad Complutense de Madrid, Madrid 28040, Spain
[c] Departamento de Análisis Matemático, Universidad de La Laguna, La Laguna, Tenerife 38271, Spain
[d] Magnetic Resonance Imaging and Spectroscopy Section, National Institute on Aging, National Institutes of Health, Baltimore, MD 21224, USA

ARTICLE INFO

Article history:
Received 1 November 2010
Revised 30 January 2011
Available online 8 March 2011

Keywords:
T_1 relaxation
T_2 relaxation
Fractional calculus
Cartilage
Extracellular matrix
Magnetic resonance imaging

ABSTRACT

We present a fractional-order extension of the Bloch equations to describe anomalous NMR relaxation phenomena (T_1 and T_2). The model has solutions in the form of Mittag–Leffler and stretched exponential functions that generalize conventional exponential relaxation. Such functions have been shown by others to be useful for describing dielectric and viscoelastic relaxation in complex, heterogeneous materials. Here, we apply these fractional-order T_1 and T_2 relaxation models to experiments performed at 9.4 and 11.7 Tesla on type I collagen gels, chondroitin sulfate mixtures, and to bovine nasal cartilage (BNC), a largely isotropic and homogeneous form of cartilage. The results show that the fractional-order analysis captures important features of NMR relaxation that are typically described by multi-exponential decay models. We find that the T_2 relaxation of BNC can be described in a unique way by a single fractional-order parameter (α), in contrast to the lack of uniqueness of multi-exponential fits in the realistic setting of a finite signal-to-noise ratio. No anomalous behavior of T_1 was observed in BNC. In the single-component gels, for T_2 measurements, increasing the concentration of the largest components of cartilage matrix, collagen and chondroitin sulfate, results in a decrease in α, reflecting a more restricted aqueous environment. The quality of the curve fits obtained using Mittag–Leffler and stretched exponential functions are in some cases superior to those obtained using mono- and bi-exponential models. In both gels and BNC, α appears to account for micro-structural complexity in the setting of an altered distribution of relaxation times. This work suggests the utility of fractional-order models to describe T_2 NMR relaxation processes in biological tissues.

1. Introduction

Experimental NMR and clinical MRI rely on accurate mathematical models for longitudinal and transverse spin relaxation [1,2]. These models are usually described by exponential functions [3,4], although it has long been recognized [5,6] that mono-exponential functions or sums of exponentials may not adequately describe NMR relaxation in complex, heterogeneous, and anisotropic materials, such as biological tissue. In these cases, the often observed stretched-exponential or power-law behavior has been described as 'anomalous' [7]. Analysis of anomalous, non-exponential, time-domain data obtained from MRS and MRI suggests the need for an alternative mathematical model to describe the relationship between relaxation processes and internal material structure. Such structures in biological tissues restrict the movement of water on multiple time and length scales, ranging from nanoseconds for the rotational correlation time to hundreds of milliseconds for T_1 relaxation. Spatial structures range from the size of a single cell to the entire length of the human spine. Fractional-order calculus [8–10] provides multi-scale mathematical models that have been used successfully to describe relaxation phenomena in polymers, dielectrics, and viscoelastic materials [11–13]. Thus, it is reasonable to consider such models in the analysis and interpretation of NMR relaxation in biological tissues.

Here we describe the development and application of a fractional-order model for NMR relaxation that leads to Mittag–Leffler and stretched exponential functions for time-domain T_1 and T_2 relaxation. These functions describe tissue complexity through fractional-order parameters that arise from operators within the

☆ Grant Sponsors: National Institute of Bioengineering and Biomedical Imaging, National Institutes of Health (NIH), Grant Number R01EB 007537, and the Intramural Research Program of the NIH, Institute on Aging.

* Corresponding author. Address: Department of Bioengineering, MC 063, Room 210, Science and Engineering Office Building, University of Illinois at Chicago, 851 South Morgan Street, Chicago, IL 60607-7052, USA. Fax: +1 312 996 5921.
E-mail address: rmagin@uic.edu (R.L. Magin).

1090-7807/$ - see front matter © 2011 Elsevier Inc. All rights reserved.
doi:10.1016/j.jmr.2011.03.006

underlying fractional-order differential equations. Such operators have been shown to reflect the distribution of relaxation times associated with tissue components (e.g., membranes and macromolecules) and compartments (e.g., vesicles, cells and extracellular matrix) in optical luminescence [16] and viscoelasticity [17,18] studies. In the present work, these functions are used to fit relaxation data obtained from mixtures of the main components of cartilage matrix, collagen and chondroitin sulfate, and from bovine nasal cartilage (BNC) [14,15]. The quality of the fit to the data is compared using the mean squared error as a metric.

In the following, we first present our fractional-order model for NMR relaxation, and then apply the resulting Mittag–Leffler and stretched exponential functions to fit T_1 and T_2 relaxation data from cartilage matrix components and native cartilage. A brief summary of the fractional calculus formalism used in this work is presented in Appendix A.

2. Theory

2.1. Bloch equations

The Bloch equation for a uniform sample can be written [19] as:

$$\frac{d\boldsymbol{M}}{dt} = \gamma \boldsymbol{M} \times \boldsymbol{B} + \frac{M_0 - M_z}{T_1}\boldsymbol{k} - \frac{M_x \boldsymbol{i} + M_y \boldsymbol{j}}{T_2} \tag{1}$$

Here, the time derivatives of the components of nuclear magnetization, $\boldsymbol{M}(t) = (M_x(t), M_y(t), M_z(t))$, are linked to the applied magnetic field $\boldsymbol{B}$ consisting of static, $\boldsymbol{B_0}$, radiofrequency, $\boldsymbol{B_1}$, and gradient field components, (G_x, G_y, G_z) by the first term on the right side. The second term describes the spin–lattice relaxation of $M_z(t)$ toward its equilibrium value of M_0 via T_1 relaxation, while the third term describes spin–spin relaxation of the $M_x(t)$ and $M_y(t)$ components through T_2 relaxation [20,21].

For a static magnetic field ($\boldsymbol{B_0} = B_0\boldsymbol{k}$) with $\omega_0 = \gamma B_0$ and a uniform sample, and defining the transverse magnetization term $M_{xy}(t) = M_x(t) + iM_y(t)$, the Bloch equations become:

$$\frac{dM_{xy}(t)}{dt} = -i\omega_0 M_{xy}(t) - \frac{M_{xy}(t)}{T_2} \tag{2a}$$

$$\frac{dM_z(t)}{dt} = \frac{M_0 - M_z(t)}{T_1} \tag{2b}$$

These differential equations can be written in an equivalent integral form as:

$$M_{xy}(t) = -i\omega_0 \int_0^t M_{xy}(\tau)d\tau - \frac{1}{T_2}\int_0^t M_{xy}(\tau)d\tau + M_{xy}(0) \tag{3a}$$

$$M_z(t) = \int_0^t \frac{M_0 - M_z(\tau)}{T_1}d\tau + M_z(0) \tag{3b}$$

The right side of Eq. (3a) can be viewed as an initial condition plus integral convolutions of the form, $k(t) * M_{xy}(t)$, with the convolution kernel $k(t) = u(t)$, and where $u(t)$ is the unit step function. Eq. (3b) has a similar structure, but with an additional constant inhomogeneous term reflecting the fact that the equilibrium solution is non-zero. The kernel $k(t)$ plays the role of a memory function that in the classical case weights all values of the magnetization equally [13]. In a complex, heterogeneous and multi-scale material where molecular interactions decay with time and distance, this simple model is more plausibly replaced by one in which the convolution kernel exhibits a 'fading' memory of earlier values of magnetization [11]. In our case, there are up to three different kernels involved: $k_0(t)$, $k_1(t)$ and, $k_2(t)$, associated with, ω_0, T_1, and T_2, respectively. We set $k_0(t) = u(t)$ for the terms affected by ω_0, reflecting the fact that Larmor precession is dominated by a constant external field and largely independent of internal material structure. Since the T_1 and T_2 relaxation terms reflect different physical processes, we allow for distinct $k_1(t)$ and $k_2(t)$.

Eqs. (3a) and (3b) can be extended to incorporate these more general convolution kernels as:

$$M_{xy}(t) = -i\omega_0 \int_0^t M_{xy}(\tau)d\tau - \frac{1}{T_2}\int_0^t k_2(t-\tau)M_x(\tau)d\tau + M_{xy}(0) \tag{4a}$$

$$M_z(t) = \int_0^t k_1(t-\tau)\frac{M_0 - M_z(\tau)}{T_1}d\tau + M_z(0) \tag{4b}$$

The exact form of the memory function kernels is unknown. A conventional choice in fractional calculus is to introduce power law kernels with fading memory in the form $k_2(t) = (t)^{\alpha-1}/\Gamma(\alpha)$, $0 < \alpha < 1$, for T_2 relaxation, and $k_1(t) = (t)^{\beta-1}/\Gamma(\beta)$, $0 < \beta < 1$, for T_1 relaxation. Substitution of these kernels into Eqs. (4a) and (4b) give fractional-order integral equations involving the Riemann–Liouville fractional integrals

$$M_{xy}(t) = -i\omega_0 \int_0^t M_{xy}(\tau)d\tau - \frac{1}{T_2^\alpha} I_{0+}^\alpha M_{xy}(t) + M_{xy}(0) \tag{5a}$$

$$M_z(t) = I_{0+}^\beta \frac{M_0 - M_z(t)}{T_1^\beta} + M_z(0) \tag{5b}$$

The definition of the fractional integral is given in Appendix A. In this formalism, $\alpha = \beta = 1$ corresponds to the classical result, leading to the conventional exponential relaxation. The extent to which these fractional-order parameters deviate from unity expresses the increasingly anomalous behavior of the T_2 and T_1 relaxation processes, respectively.

2.2. Fractional-order Bloch equations

To revert to the equivalent differential form, we apply the fractional derivatives of order α and β to Eqs. (5a) and (5b), respectively, obtaining the following form for the fractional-order components of the Bloch equation:

$$D_{0+}^\alpha M_{xy}(t) = -i\omega_0 I_{0+}^{1-\alpha} M_{xy}(t) - \frac{1}{T_2^\alpha} M_{xy}(t) + D_{0+}^\alpha M_{xy}(0) \tag{6a}$$

$$D_{0+}^\beta M_z(t) = \frac{M_0 - M_z(t)}{T_1^\beta} + D_{0+}^\beta M_z(0) \tag{6b}$$

Here, the fractional derivatives are expressed as Riemann–Liouville fractional derivative operators (see Appendix A). Since the initial conditions specified in a particular NMR experiment involve fractional derivatives of the magnetization evaluated at $t = 0^+$, an equivalent form can be written in terms of the Caputo fractional derivative (see Appendix A).

$${}^C D_{0+}^\alpha M_{xy}(t) = -i\omega_0 I_{0+}^{1-\alpha} M_{xy}(t) - \frac{1}{T_2^\alpha} M_{xy}(t) \tag{7a}$$

$${}^C D_{0+}^\beta M_z(t) = \frac{M_0 - M_z(t)}{T_1^\beta} \tag{7b}$$

The solution to this set of equations provides a generalized, fractional-order response that extends the classical exponential relaxation processes [22,23]. We will briefly describe the most relevant results of this new model for the dynamics of NMR phenomena.

2.3. Fractional-order T_1 relaxation

The solution to Eqs. (5b), (7b) can be obtained using fractional calculus or the Laplace transformation [24]:

$$M_z(t) = M_z(0) + [M_0 - M_z(0)][1 - E_\beta(-(t/T_1)^\beta)] \quad (8)$$

where E_β is the stretched Mittag–Leffler function (see Appendix A). In the case of $\beta = 1$, the Mittag–Leffler function is equivalent to the simple exponential function and the classical expression for T_1 relaxation emerges. For small values of the argument (t/T_1), the stretched Mittag–Leffler function converges to the stretched exponential $\exp[-(t/T_1)^\beta]$, where β is the stretching parameter. For an inversion recovery pulse sequence, the inversion time TI becomes the time argument, $M_z(0) = -M_0$, and, accounting for potential imperfections in the inversion pulse by a proportionality constant A [25], M_z is given by:

$$M_z(TI) = M_0[1 - 2AE_\beta(-(TI/T_1)^\beta)] \quad (9)$$

Eq. (9) is plotted in Fig. 1 showing the return of M_z to its equilibrium value of one as a function of TI for $T_1 = 1.5$ s, $A = 1$ and for values of β from 0.6 to 1.0, in steps of 0.1. For $\beta = 1$ we recover the classical single exponential relaxation. For smaller values of β the relaxation appears to occur more slowly for larger values of TI. Thus, we observe that the fractional-order dynamic model for M_z introduces a feature that is usually observed in multi-exponential models by an apparent lengthening of the relaxation time as relaxation progresses. It is important to note that this relaxation behavior is different from the conventional case even for beta as large as 0.9.

2.4. Fractional-order T_2 relaxation

In a similar manner, using fractional calculus or the Laplace transform, we obtain the solution to Eqs. (5a), (7a) for a single $\pi/2$ pulse in a reference frame rotating with an angular frequency ω_0 and in the presence of noise with a non-zero mean as:

$$M_{xy}(TE) = M_{xy}(0)E_\alpha[-(TE/T_2)^\alpha] + M_{xy}(\infty) \quad (10)$$

Eq. (10) is plotted in Fig. 2 as a function of TE with $M_{xy}(0) = 1$ and $M_{xy}(\infty) = 0.05$ for values of α from 0.6 to 1.0, in steps of 0.1 and for a T_1 value of 80 ms. In Fig. 2, the vertical scale is logarithmic, so that the initial sections of the decay curves appear as straight lines. Decreasing the value of α extends the decay curve so that it exhibits a longer apparent T_2. In the fractional-order case of T_2 relaxation, Eq. (10), the stretched Mittag–Leffler function or the stretched exponential replaces the single exponential function.

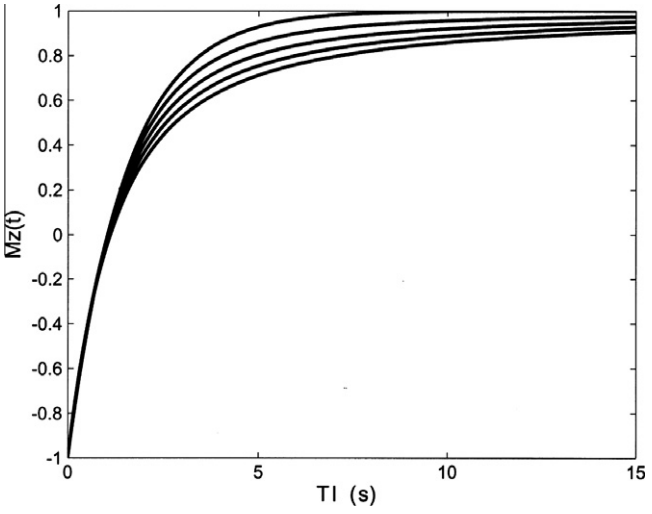

Fig. 1. Fractional-order T_1 relaxation curves. Plots of $M_z(TI)$ versus TI (Eq. (9)) for different values of β in the range from $\beta = 0.6$ (bottom curve) to $\beta = 1$ in steps of 0.1 ($M_0 = 1$, $T_1 = 1.5$ s, $A = 1$).

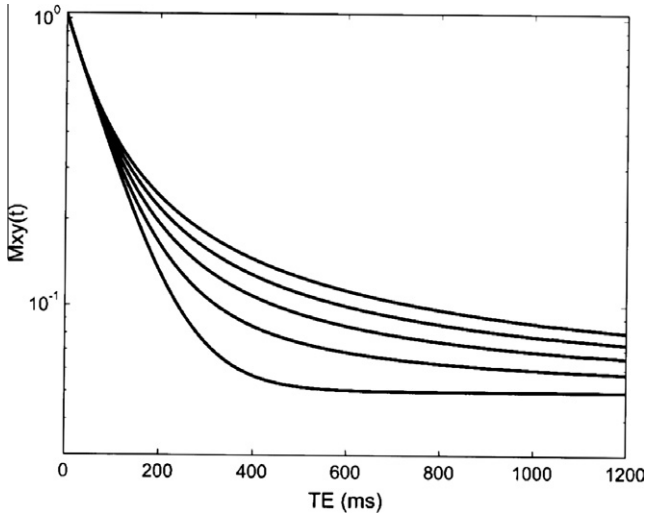

Fig. 2. Fractional-order T_2 relaxation curves. Plots of $M_{xy}(TE)$ versus TE (Eq. (10)) for different values of α in the range from $\alpha = 0.6$ (top curve) to $\alpha = 1$ in steps of 0.1 ($M_{xy}(0) = 1$, $T_2 = 80$ ms, $M_{xy}(\infty) = 0.05$).

3. Methods

3.1. Type I collagen gels

Collagen I solution (rat tail tendon, BD Biosciences, San Jose, CA) was prepared according to the manufacturer's instructions to a concentration of 2.7 mg/ml. 3 ml volumes of this solution were transferred into NMR tubes, allowed to gel at 37 °C, and concentrated using centrifugation at 2500*g* for up to 2.5 h. Gels with a range of collagen concentrations were constructed in this fashion. Final concentrations were determined by subtraction of the supernatant contribution from the original weight, and were 0%, 0.65%, and 2.42%.

3.2. Chondroitin sulfate mixtures

Dry chondroitin sulfate (shark cartilage, Sigma–Aldrich St. Louis, MO) was dissolved in 10× PBS to make 5%, 10%, and 15% solutions. Although chondroitin sulfate is highly soluble, great care was taken not to form air bubbles while mixing.

3.3. BNC preparation

Cartilage plugs (4 mm or 8 mm dia.) were excised from the nasal septa of mature cows (Green Village Packing, Green Village, NJ), moistened with Dulbecco's phosphate buffered saline (DPBS) and stored at 4 °C.

3.4. NMR methods

All non-localized T_1 relaxation data, T_1 imaging data, and T_2 imaging data were acquired at room temperature using an 11.7 T Bruker NMR spectrometer (Bruker BioSpin, Billerica, MA). BNC (4 mm dia. plug) was placed into a 5 mm NMR tube containing Fluorinert (FC-43, 3M, St. Paul, MN) to maintain sample hydration and preclude MR signal contamination from the bath solution. Non-localized T_1 relaxation data were obtained using an inversion

recovery pulse sequence (180-TI-90) with 64 linearly spaced *TI*s from 0 to 15 s. MR images of BNC were obtained using a single slice of 0.3 mm thickness, with field-of-view of 6.4 mm × 6.4 mm and in-plane resolution of 50 μm × 50 μm. Quantitative T_1 maps were obtained using a progressive saturation spin echo sequence with TE = 10 ms and 16 linearly spaced TRs from 100 ms to 10 s. Quantitative T_2 maps were obtained using a CPMG sequence with 16 linearly spaced echoes, with TE = 7.2 ms and TR = 4 s.

All non-localized T_2 relaxation data were acquired at room temperature for matrix component mixtures and 4 °C for BNC samples (8 mm dia. plug) with a 9.4 T Bruker DMX NMR spectrometer (Bruker BioSpin, Billerica, MA). BNC (8 mm diameter plug) was placed into a 10 mm NMR tube containing Fluorinert. T_2 relaxation data were obtained on BNC samples using a non-localized CPMG pulse sequence with the following acquisition parameters: TR/TE = 600 μs/10 s, 2048 echoes, and NEX = 64, with sampling of the echo maxima. This resulted in a single decay curve representing the entire sample in bulk. T_2 relaxation data obtained on collagen and chondroitin sulfate mixtures were acquired using the same parameters but with 8192 echoes. Even echoes were used for T_2 fitting resulting in an effective TE = 1.2 ms, with 1024 echoes for BNC and 4096 echoes for matrix component mixtures.

3.5. Data analysis

All data fits (exponential, Mittag–Leffler and stretched exponential functions) were preformed in Matlab (The MathWorks, Natick, MA) using the FIT routine. The Mittag–Leffler function, E_α, was fit using the Diethelm approximation [26]. The mean squared error (MSE) – the square root of the sum of the squared differences between actual data and fitted curve – is reported for each model. Note that given the experimental protocols described, the independent time variables in the equations describing relaxation become TE and TI.

4. Results

Table 1 provides a comparison between the fractional-order models and the single exponential function for fits of T_2 relaxation in solutions of type I collagen gels. All three functions show decreasing values of T_2 with increasing concentration of collagen. The stretched exponential function and the stretched Mittag–Leffler function also show decreases in the parameter α as the collagen concentration increases. The stretched exponential spans the largest dynamic range of α (from 1.0 to 0.89), while the stretched Mittag–Leffler function extends only from 1.0 to 0.96. Over the range of concentrations studied, the MSE was the smallest for the stretched exponential function and largest for the single exponential.

Table 2 shows a similar comparison between the fractional-order models and the single exponential function for fits of T_2 relaxation for chondroitin sulfate solutions. All functions showed a decrease in T_2 with increasing chondroitin sulfate concentration.

Table 1
Fractional-order model fitting results of T_2 relaxation data from collagen I gels.

Conc. (%)	Exponential		Stretched MLF			Stretched exponential		
	T_2 (ms)	MSE ($\times 10^{-3}$)	T_2 (ms)	α	MSE ($\times 10^{-3}$)	T_2 (ms)	α	MSE ($\times 10^{-3}$)
0	2867	3.47	2867	1	3.47	2867	1	3.47
0.65	1307	3.53	1326	0.97	1.04	1305	0.94	0.83
2.42	493	6.80	487	0.96	3.27	475	0.89	1.45

All three models show a decrease in T_2 and both fractional models show decreasing α with increasing collagen concentration.

Table 2
Fractional-order model fitting results of T_2 relaxation data from chondroitin sulfate mixtures.

Conc. (%)	Exponential		Stretched MLF			Stretched exponential		
	T_2 (ms)	MSE ($\times 10^{-3}$)	T_2 (ms)	α	MSE ($\times 10^{-3}$)	T_2 (ms)	α	MSE ($\times 10^{-3}$)
0	2867	3.47	2867	1	3.47	2867	1	3.47
5	390	1.93	391	0.99	1.43	390	0.97	0.94
10	220	2.92	218	0.99	2.27	216	0.96	1.25
15	167	4.19	165	0.99	3.28	161	0.94	3.05

All three models show a decrease in T_2 with increasing concentration of chondroitin sulfate mixtures. The stretched exponential model shows a decrease in the fractional-order parameter α.

Consistent with the collagen results, the fractional-order parameter for the stretched exponential fits showed a greater sensitivity to concentration than did the stretched Mittag–Leffler model, with α ranging from 1 to 0.94 for chondroitin sulfate concentrations of 0–15%, respectively. The stretched Mittag–Leffler fit did not show any change in α with concentration. The stretched exponential fit also showed the lowest MSE of all three models.

The microstructure of the BNC is evident in the T_1-weighted and T_2-weighted MR images shown in Fig. 3A and B, respectively. The corresponding spatial maps for the mono-exponential T_1 and the T_2 distributions in this 0.3 mm thick slice are shown in Fig. 3C and D, respectively. These images show a small blood vessel (diameter of approximately 500 μm) in the nine o'clock position. Small and sparse capillaries can be found in young nasal cartilage. Capillary density is reduced with development. The overall contrast appears to be greater in the T_2 images than in the T_1 images, indicating a wider range of relaxation times in the underlying tissue environments.

Tables 3 shows fractional-order and exponential T_1 curve fit parameters and MSE for non-localized T_1 relaxation data in BNC. In all cases the A value was essentially the same (0.91 or 0.92). For this BNC sample the T_1 data was well described by a single exponential function with a T_1 of 1.68 s. The bi-exponential fit reduced the MSE and introduced an apparent shorter T_1 component (T_1 = 1.12 s) that may not have been sufficiently different from the longer component to be reliably distinguished. The fractional-order functions in this case were very similar to the single exponential results with values of α very close to one (0.98 and 0.99) and T_1 values of 1.66 and 1.67 s, for the stretched exponential and MLF fits, respectively. Both the exponential and the stretched exponential models showed an excellent fit to the data. The quality of the T_1 curve fits for BNC can be observed graphically in Fig. 4, which shows results consistent with those in Table 3 with the single exponential and the stretched exponential models.

Table 4 shows fractional-order and exponential T_2 curve fit parameters and MSE for non-localized T_2 relaxation data in BNC. The stretched exponential model shows the lowest MSE of all the fits in spite of having fewer fitting parameters. Fig. 5 shows the improvement in fit of T_2 relaxation data when using the stretched exponential.

5. Discussion and conclusions

Previous NMR studies have found that fractional-order models provide excellent results when used to describe dynamic processes in complex media, such as NMR diffusion in porous materials [4], and human brain tissue [22,27]. In this paper we fit relaxation data obtained using cartilage matrix components and BNC to stretched exponential and stretched Mittag–Leffler functions derived from a fractional-order generalization of the Bloch equation. BNC is ideal for this analysis because it is heterogeneous over the micro-scale,

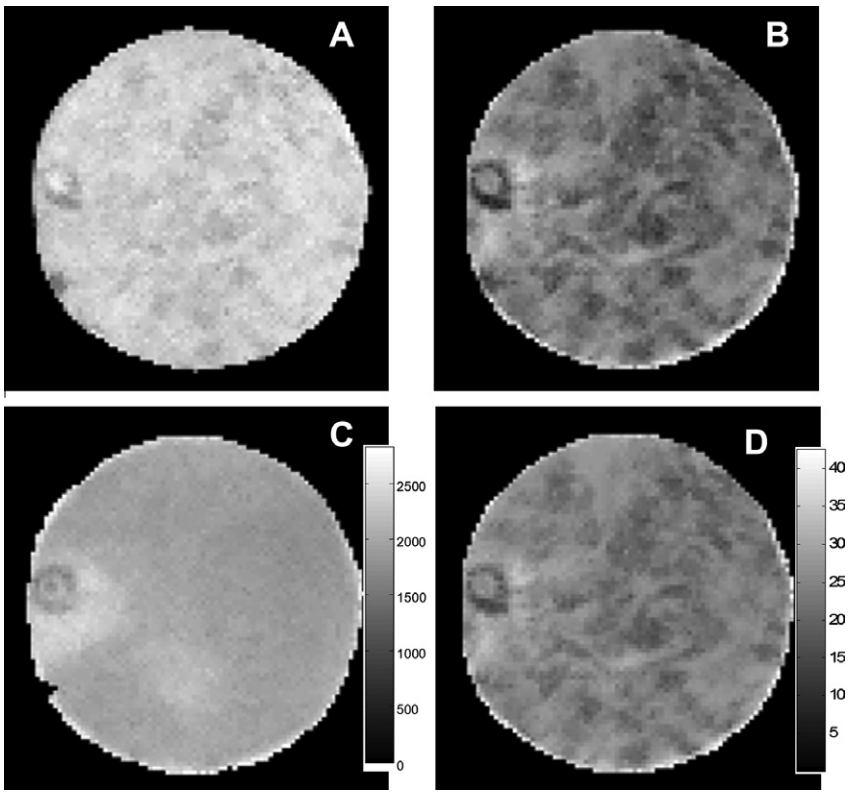

Fig. 3. MR images of bovine nasal cartilage (BNC). (A) T_1 – weighted image with TR/TE = 500/9.8 ms, FOV = 6.4 mm × 6.4 mm, slice thickness of 0.3 mm and in-plane resolution of 50 μm × 50 μm; (B) T_2 – weighted image with TR/TE = 4000/28.8 ms, FOV = 6.4 mm × 6.4 mm, slice thickness of 0.3 mm and in-plane resolution of 50 μm × 50 μm; (C) T_1 map for the slice shown in (A) showing mono-exponential T_1 relaxation (gray scale: T_1, 0–2500 ms); (D) T_2 map for the slice shown in (B) showing mono-exponential T_2 relaxation (gray scale: T_2, 0–40 ms).

Table 3
Multiple exponential and fractional-order model fitting results for T_1 relaxation data from BNC.

Model	A	a_1	a_2	T_{11} (s)	T_{12} (s)	β	MSE ($\times 10^{-3}$)
1-exp	0.91	1.00		1.68			6.2
2-exp	0.92	0.84	0.16	1.80	1.12		1.8
str exp	0.92	1.00		1.66		0.98	4.8
str MLF	0.91	1.00		1.67		0.99	5.5

The fitting parameter A represents a correction for an imperfect inversion pulse, while a_n and T_{1n} represent the relative compartment size and longitudinal relaxation time of the nth longitudinal relaxation component.

as is all tissue, but relatively homogeneous over the scale of the imaging voxel. Thus, the presence of multiple relaxation environments for water, including relatively free tissue water, water closely bound to proteoglycans, and water loosely bound to macromolecules, can be investigated without the complexity of accounting for overall variation in tissue properties [28–31]. We hypothesized that, due to these micro-structural features, relaxation processes in BNC would display a distribution of relaxation times [32,33] that can be characterized by fractional-order models.

In this paper we derived a generalized model for the dynamics of a single species in NMR by assuming a fractional-order fading memory kernel (e.g., $\{(t)^{(\alpha-1)}/\Gamma(\alpha)\}$). This extension of the Bloch equations adds memory, via convolution, to the classical model, but retains linearity, causality, and time-invariance The underlying physical picture is therefore modified by the introduction of an arbitrarily long, non-exponential, correlation function. Thus, the fractional-order generalization of NMR represents a natural extension of the conventional approach in which relaxation processes occur independently of previous states. Indeed, as the fractional-order parameters approach unity, relaxation dynamics converges to the classical results.

There are a number of options available for defining the fractional-order time derivative (e.g., Riemann–Liouville, Caputo, Grunwald–Letnikov) [34]. The most common approach is to select the Caputo definition for systems like NMR where there are clearly defined initial conditions [23]. In general, different fractional power laws are expected for T_1 and for T_2 relaxation. Our final mathematical result is a sinusoidal oscillating decay governed by a stretched Mittag–Leffler relaxation function. This new approach identifies separate fractional orders (α, β) for spin–spin and spin–lattice relaxation processes, respectively. One key aspect of this new model is that the signal attenuation is now assumed to proceed in the rotating frame as a pure fractional-order decay process, as also observed in other fractional-order generalizations of physical and chemical processes [6,11,13]. In this paper, we have focused on experimental fitting of the fractional-order model for relaxation via both the single parameter stretched Mittag–Leffler function, and the stretched exponential.

In our analysis of gels (collagen type I and chondroitin sulfate) we established the expected correlation between polymer concentration and T_2 relaxation time. In addition, we found that the fractional-order parameter α was sensitive to gel concentration, decreasing with gel concentration for both gels. It was somewhat unexpected that the fractional-order parameter for the stretched exponential decay curve fits were more sensitive to increasing gel concentration than those obtained using the Mittag–Leffler function. However, it is well known that the Mittag–Leffler function interpolates between the stretched exponential (at small values of its argument) and the power law (at large values), while both functions decay quite differently from the single exponential [10,13]. Thus, the fact that the data collected for gels (and for BNC)

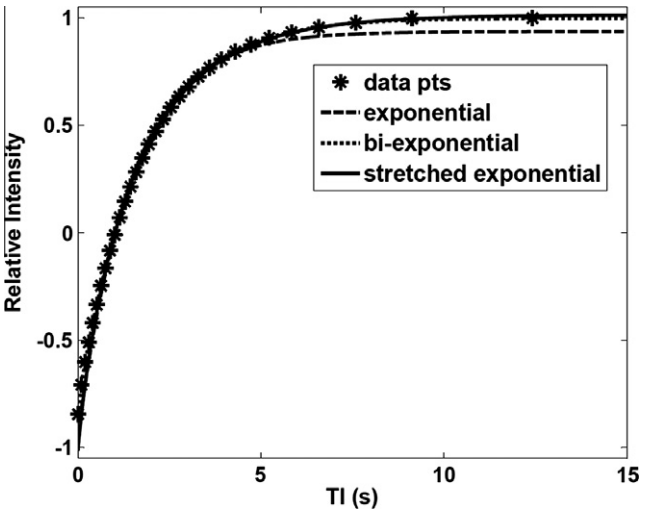

Fig. 4. T_1 relaxation data fits for BNC. The experimental data (*) with the corresponding fits by a single exponential function (long-dashed line), a bi-exponential function (short-dashed line), and a stretched exponential function (solid line). The displayed data points (*) represent a subset of the 64 total relaxation decay points.

Table 4
Multiple exponential and fractional-order model fitting results for T_2 relaxation data from BNC.

Model	a_0 ($\times 10^{-3}$)	a_1	a_2	T_{21} (ms)	T_{22} (ms)	α	MSE ($\times 10^{-3}$)
1-exp	6.30	1.00		87.3			5.5
2-exp	4.20	0.77	0.23	100.8	34.1		0.84
str exp	3.80	1.00		79.7		0.88	0.13
str MLF	0.00	1.00		83.0		0.96	2.4

The fitting parameters a_n and T_{2n} represent the relative compartment size and transverse relaxation time of the nth transverse relaxation component, while a_0 corresponds to a constant offset term, represented by $M_{xy}(\infty)$ in Eq. (10).

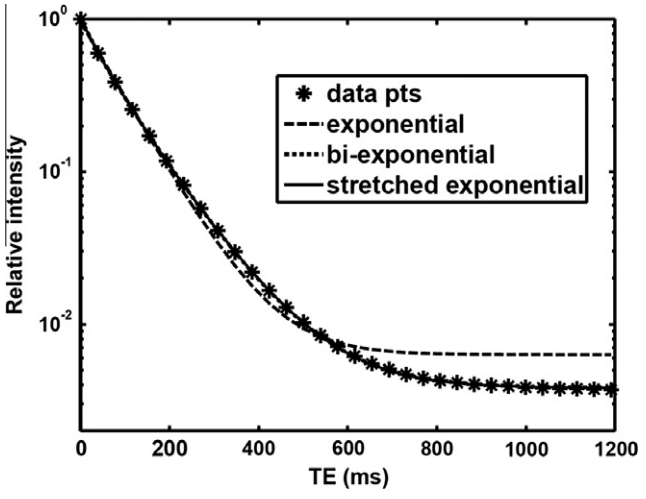

Fig. 5. T_2 relaxation data fits for BNC. The experimental data (*) with the corresponding fits by a single exponential function (long-dashed line), a bi-exponential function (short-dashed line), and a stretched exponential function (solid line). The displayed data points (*) represent a subset of the total 4096 relaxation decay points.

is better fit by the stretched exponential model than the Mittag–Leffler function (lower MSE) and is more sensitive to the fractional-order parameter (larger change in α) possibly reflects the greater sensitivity of the stretched exponential function to the earlier part of the T_2 decay curve than the later part.

In our analysis of BNC we compared the conventional multi-compartment, multi-exponential models for T_1 and T_2 relaxation with the single compartment fractional-order generalization. In the case of T_1 relaxation, we found no advantage in fitting the data using the fractional-order function. In fact, one feature of this approach is that in such cases the value of the parameter β closely approaches the classical value of one. In this example, using BNC, the fitting data for the stretched exponential and the stretched Mittag–Leffler function gave values for β of 0.98 and 0.99, respectively. The MSE for fits to the BNC T_1 were approximately the same, as were also the T_1 values (1.67 s). The mono-exponential behavior of T_1 relaxation is consistent with exchange between tissue compartments occurring within the slow time-scale of T_1 processes. In the case of T_2 relaxation, we found an advantage to fitting the data with multi-exponential and fractional-order models. With a_n designating the relative size and T_{2n} designating the transverse relaxation time of the nth compartment in a multi-compartment system, the values of these parameters and of α resulting from best fits to the observed data could prove to be of use in quantitative tissue analysis. Also, parameter values obtained proved to be independent of the initial values used for repeated fitting trials (data not shown).

Multi-exponential models exhibit a straightforward interpretation in terms of compartmental analysis: each individual relaxation function corresponds to the water molecules in a distinct tissue environment, a_n, that exhibits a single relaxation process described by the time constant T_{2n}. Multi-exponential results obtained using the TEs indicated can therefore be interpreted in terms of a model of BNC as consisting of two dominant populations of water undergoing either fast, or slow relaxation. For the BNC studies as presented here, this interpretation corresponds to a 23% rapidly relaxing component (T_2 = 34 ms, for water associated with macromolecules), and a 77% slowly relaxing component (T_2 = 101 ms, for highly mobile water not closely bound to ECM components. This interpretation is consistent with previous multi-exponential relaxation studies of cartilage [14]. The stretched exponential function captures this structural information in an intermediate T_2 value of 80 ms and a fractional-order parameter, α, of 0.88. In the case of the matrix component solutions, increasing concentration resulted in a reduction in bulk T_2. Thus, it appears that at least part of the observed fractional-order behavior in BNC is associated with water characteristics at the molecular level, with the remainder associated with the multi-scale structure of the overall tissue. We note that our highest collagen concentration was still only about 10% of that found in the native cartilage, so we might anticipate even larger changes in the fractional parameters in more rigid gels.

The fractional calculus approach to modeling NMR relaxation is to incorporate tissue complexity not through multiple compartments, but in the order of the assumed fractional operator. This permits the data to be fit accurately with a smaller number of functions, removing at least in part the degeneracy of multi-exponential discrete compartmental models. This approach also has a structural basis when the tissue exhibits a self-similarity that can be described by a fractal dimension [35,36]. Since the order of the fractional operator can be connected with the fractal features of the tissue, the fractional model also provides a representation of a complex tissue not as a series of compartments and relaxation times, but as a single generalized exponential function in terms of α and T_2 or β and T_1. Such models have been recently applied to the attenuation of acoustic waves in random multi-scale media [37,38] viscoelasticity [39,40] and to NMR analysis of diffusion in porous media [41–46].

For complex systems such as biological tissue, we propose consideration of the fractional-order approach as an alternative to discrete-compartment exponential models. The approach developed in this paper captures structural features via pairs of tissue-dependent parameters: (T_2, α) or (T_1, β). Fractional-order generalization of the Bloch equation provides a sound foundation for this technique. The method is, for the tissue considered in this work, at least as effective at fitting the data as a bi-exponential analysis, when assessed by the MSE of the relaxation curve fits. As a further extension, the inverse Laplace transformation can yield a distribution of relaxation times corresponding to the fractional parameter in the stretched exponential and the stretched Mittag–Leffler functions, as has been done by Berberan-Santos [16] and others in the analysis of the time decay of optical luminescence data. When the α-value deviates from unity, for example, the distribution of relaxation rates (or times) broadens. While using a single function to encode tissue complexity may be an oversimplification, for BNC we observed a good correspondence between our model and the T_2 relaxation results.

Further work will define the utility and specificity of the approach presented here for detecting changes in the composition of tissue as a consequence of degradation processes, such as are seen in degenerative joint disease. A particular goal will be to correlate changes in the tissue parameters α and β with histological and biochemical analysis of tissue samples. The present work shows the plausibility of this approach.

Acknowledgments

R.L. Magin would like to acknowledge the support of NIH Grant R01 EB007537 for partial support of this work. D.A. Reiter and R.G. Spencer would like to acknowledge the support of the Intramural Research Program of the NIH, National Institute on Aging. J. Trujillo and M.P. Velasco would like to acknowledge support for this work, in part, from the MICINN of Spain (Grants MTM2007-60246 and MTM2010-16499).

Appendix A. Fractional integral and differential operators

Fractional calculus extends the classical definitions of the derivative and the integral, introducing intermediate, non-integer orders. The physical basis for its application in physics is described in two review papers written by R. Metzler and J. Klafter [47,48]. There are several definitions of fractional derivatives and integrals; here we introduce the operators used in this work and some of their properties (see also [10,24,34]).

(1) *Riemann–Liouville fractional operators*: Let $\alpha > 0$ with $n-1 < \alpha < n$ for integer values of n, let $f(t)$ be a suitable real function of t on the interval $[a, b]$ such that the fractional integral exists [24,34].

$$(I^{\alpha}_{a+}f)(t) = \frac{1}{\Gamma(\alpha)}\int_a^t (t-\tau)^{\alpha-1} f(\tau)\,d\tau \quad (t > a) \tag{A.1a}$$

$$(D^{\alpha}_{a+}f)(t) = D^n(I^{n-\alpha}_{a+}f)(t) \quad (t > a) \tag{A.1b}$$

where $\Gamma(\alpha)$ is the gamma function, and D is the usual differential operator. The fractional-order integrals can also be defined in terms of the convolution of $t^{(\alpha-1)}/\Gamma(\alpha)$ with $f(t)$ [13].

(2) *Caputo fractional derivative*: Let $\alpha > 0$ with $n-1 < \alpha < n$ for integer values of n, let $f(t)$ be a suitable real function of t on the interval $[a, b]$ such that the fractional integral exists [24,34].

The Caputo fractional derivative is:

$$({}^{C}D^{\alpha}_{a+}f)(t) = I^{n-\alpha}_{a+}(D^n f)(t) \quad (t > a) \tag{A.2}$$

The change in the order of operations does not affect the order α, but it does restrict the space of integrable functions. Another consequence for fractional-order differential equations is that the initial conditions can now be specified in terms of the initial values of $f(t)$, whereas the Riemann–Liouville definition calls for initial values of the fractional integral of $f(t)$. The following identity is well known for a suitable function $f(t)$ (for example, $f(t)$ is n-times differentiable):

$$(D^{\alpha}_{a+}f)(t) = ({}^{C}D^{\alpha}_{a+}f)(t) + \sum_{j=0}^{n-1}\frac{f^{(j)}(a)}{\Gamma(1+j-\alpha)}(t-a)^{j-\alpha} \tag{A.3}$$

(3) *Mittag–Leffler function (single parameter):*

$$E_{\alpha}(z) = \sum_{k=0}^{\infty}\frac{z^k}{\Gamma(\alpha k+1)} \quad (\alpha > 0) \tag{A.4}$$

This function is a generalization of the classical exponential function (when α is one). The stretched Mittag–Leffler function has the following property:

$${}^{C}D^{\alpha}_{0+}E_{\alpha}(\lambda t^{\alpha}) = \lambda E_{\alpha}(\lambda t^{\alpha}) \tag{A.5}$$

which mimics the behavior of the ordinary derivative operating on the exponential function. Finally, the single parameter stretched Mittag–Leffler function has the following asymptotic behavior for small and for large values of its argument [10,35].

$$E_{\alpha}(-t^{\alpha}) = 1 - t^{\alpha}/\Gamma(1+\alpha) \quad t \to 0^{+} \tag{A.6}$$

$$E_{\alpha}(-t^{\alpha}) = t^{-\alpha}/\Gamma(1-\alpha) \quad t \to \infty \tag{A.7}$$

Thus, initially the stretched Mittag–Leffler function decays like the power series expansion of the stretched exponential function, $\exp(-t^{\alpha}/\Gamma(1+\alpha))$, while for long times it fall off as a simple power law. This behavior is clearly illustrated in Fig. 22 on page 62 of Ref. [47] and by Fig. 7 on page R177 of Ref. [48].

References

[1] A. Abragam, Principles of Nuclear Magnetism, Oxford University Press, New York, 2002.
[2] E.M. Haacke, R.W. Brown, M.R. Thompson, R. Venkatesan, Magnetic Resonance Imaging: Physical Principles and Sequence Design, John Wiley and Sons, New York, 1999.
[3] E.D. Becker, High Resolution NMR: Theory and Chemical Applications, third ed., Academic Press, San Diego, 2000.
[4] P.T. Callaghan, Principles of Magnetic Resonance Microscopy, Oxford University Press, Oxford, 1991.
[5] R. Lenk, Brownian Motion and Spin Relaxation, Elsevier, Amsterdam, 1977.
[6] R. Kimmich, Strange kinetics, porous media, and NMR, Chem. Phys. 284 (2002) 253–285.
[7] A.E. Sitnitsky, G.G. Pimenov, A.V. Anisimov, Spin-lattice NMR relaxation by anomalous translational diffusion, J. Magn. Reson. 172 (2005) 48–55.
[8] K.B. Oldham, J. Spanier, The Fractional Calculus: Theory and Applications of Differentiation and Integration to Arbitrary Order, Academic Press, New York, 1974.
[9] S.G. Samko, A.A. Kilbas, O.I. Marichev, Fractional Integrals and Derivatives: Theory and Applications, Gordon and Breach, Switzerland, 1993.
[10] A.A. Kilbas, H.M. Srivastava, J.J. Trujillo, Theory and Application of Fractional Differential Equations, Elsevier, Amsterdam, 2006.
[11] R. Hilfer (Ed.), Applications of Fractional Calculus in Physics, World Scientific, Singapore, 2000.
[12] B.J. West, M. Bolgona, P. Grigolini, Physics of Fractal Operators, Springer-Verlag, New York, 2003.
[13] R.L. Magin, Fractional Calculus in Bioengineering, Begell House, Connecticut, 2006.
[14] D.A. Reiter, P.C. Lin, K.W. Fishbein, R.G. Spencer, Multicomponent T2 relaxation analysis in cartilage, Magn. Reson. Med. 61 (2009) 803–809.
[15] P.C. Lin, D.A. Reiter, R.G. Spencer, Classification of degraded cartilage through multi-parametric MRI analysis, J. Magn. Reson. 201 (2009) 61–71.
[16] M. Berberan-Santos, E.N. Bodunov, B. Valeur, Luminescence decays with underlying distributions of rate constants: General properties and selected cases, in: M.N. Berberan-Santos (Ed.), Fluorescence of Supermolecules, Polymers, and Nanosystems, Springer, Berlin, 2008, pp. 67–103.
[17] R.S. Lakes, Viscoelastic Solids, CRC Press, Boca Raton, 1998.

[18] Y.C. Fung, Biomechanics: Mechanical Properties of Living Tissues, second ed., Springer, New York, 1993.
[19] Z.P. Liang, P.C. Lauterbur, Principles of Magnetic Resonance Imaging: A Signal Processing Perspective, IEEE Press, New York, 2000.
[20] M.A. Bernstein, K.F. King, X.J. Zhou, Handbook of MRI Pulse Sequences, Elsevier Academic Press, Burlington, 2004.
[21] M.T. Vlaardingerbroek, J.A. den Boer, Magnetic Resonance Imaging, second ed., Springer- Verlag, Berlin, 1999.
[22] R.L. Magin, O. Abdullah, D. Baleanu, X.J. Zhou, Anomalous diffusion expressed through fractional order differential operators in the Bloch-Torrey equation, J. Magn. Reson. 190 (2008) 255–270.
[23] R.L. Magin, X. Feng, D. Baleanu, Fractional calculus in NMR, Magn. Reson. Eng. 34 (2009) 16–23.
[24] I. Podlubny, Fractional Differential Equations, Academic Press, New York, 1999.
[25] R. Freeman, A Handbook of Nuclear Magnetic Resonance, Wiley, New York, 1988.
[26] K. Diethelm, N.J. Ford, A.D. Freed, Y.F. Luchko, Algorithms for the fractional calculus: a selection of numerical methods, Comput. Meth. Appl. Mech. Eng. 194 (2005) 743–777.
[27] X.J. Zhou, Q. Gao, O. Abdullah, R.L. Magin, Studies of anomalous diffusion in the human brain using fractional order calculus, Magn. Reson. Med. 63 (2010) 562–569.
[28] N.M. Menezes, M.L. Gray, J.R. Hartke, D. Burstein, T-2 and T1, MRI in articular cartilage systems, Magn. Reson. Med. 51 (2004) 503–509.
[29] D.S. Grebenkov, Use, misuse, and abuse of apparent diffusion coefficients, Conc. Magn. Reson. 36A (2009) 24–35.
[30] G. Blumenkrantz, J. Zuo, X. Li, J. Kornak, T.M. Link, S. Majumdar, In vivo 3.0-Tesla magnetic resonance T_1rho and T_2 relaxation mapping in subjects with intervertebral disc degeneration and clinical symptoms, Magn. Reson. Med. 63 (2010) 1193–1200.
[31] R.R. Regatte, S.V. Akella, J.H. Lonner, R. Reddy, $T_{1\rho}$ relaxation mapping in human osteoarthritis (OA) cartilage: comparison of $T_{1\rho}$ with T_2, Magn Reson. Imag. 23 (2006) 547–553.
[32] R.M. Mazo, , Brownian Motion: Fluctuations, Dynamics, and Applications, Oxford University Press, Oxford, 2002.
[33] K.D. Whittall, A.L. MacKay, Quantitative interpretation of NMR relaxation data, J. Magn. Reson. 84 (1989) 134–152.
[34] K. Diethelm, The Analysis of Fractional Differential Equations, Springer, NewYork, 2010.
[35] A. Carpinteri, F. Mainardi (Eds.), Fractals and Fractional Calculus in Continuum Mechanics CISM Courses and Lectures No. 378, Springer-Wien, New York, 1997.
[36] R. Kopelman, Fractal reaction kinetics, Science 241 (1988) 1620–1626.
[37] J. Garnier, K. Soina, Effective fractional acoustic wave equations in one-dimensional random multiscale media, J. Acoust. Soc. Am. 127 (2010) 62–72.
[38] S. Holm, R. Sinkus, A unifying fractional wave equation for compressional and shear waves, J. Acoust. Soc. Am. 127 (2010) 542–548.
[39] W.G. Gloeckle, T.F. Nonnenmacher, Fractional integral operators and Fox functions in the theory of viscoelasticity, Macromolecules 24 (1991) 6426–6434.
[40] R. Metzler, W. Schick, H.-G. Kilian, T.F. Nonnenmacher, Relaxation in filled polymers: a fractional calculus approach, J. Chem. Phys. 103 (1995) 7180–7186.
[41] R. Kimmich, NMR Tomography, Diffusion, Relaxometry, Springer, Berlin, 1997. pp. 183–187.
[42] J.R. Banavar, M. Lipsicas, J.F. Willemsen, Determination of the random-walk dimension of fractals by means of NMR, Phys. Rev. B 32 (1985) 5575–6112.
[43] G. Jug, Theory of NMR field-gradient spectroscopy for anomalous diffusion in fractal networks, Chem. Phys. Lett. 131 (1986) 94–97.
[44] J. Kärger, G. Vojta, On the use of NMR pulsed field-gradient spectroscopy for the study of anomalous diffusion in fractal networks, Chem. Phys. Lett. 141 (1987) 411–413.
[45] J. Kärger, H. Pfeifer, G. Vojta, Time correlation during anomalous diffusion in fractal systems and signal attenuation in NMR field-gradient spectroscopy, Phys. Rev. A 37 (1988) 4514–4517.
[46] A. Widom, H.J. Chen, Fractal Brownian motion and nuclear spin echoes, J. Phys. A 28 (1995) 1243–1247.
[47] R. Metzler, J. Klafter, The random walk's guide to anomalous diffusion: a fractional dynamics approach, Phys. Repts. 339 (2000) 1–77.
[48] R. Metzler, J. Klafter, The restaurant at the end of the random walk: recent developments in the description of anomalous transport by fractional dynamics, J. Phys. A: Math. Gen. 37 (2004) R161–R208.